

Unabated planetary warming and its ocean structure since 2006

Dean Roemmich^{1*}, John Church², John Gilson¹, Didier Monselesan², Philip Sutton³ and Susan Wijffels²

Increasing heat content of the global ocean dominates the energy imbalance in the climate system¹. Here we show that ocean heat gain over the 0–2,000 m layer continued at a rate of 0.4–0.6 W m⁻² during 2006–2013. The depth dependence and spatial structure of temperature changes are described on the basis of the Argo Program's² accurate and spatially homogeneous data set, through comparison of three Argo-only analyses. Heat gain was divided equally between upper ocean, 0–500 m and 500–2,000 m components. Surface temperature and upper 100 m heat content tracked interannual El Niño/Southern Oscillation fluctuations³, but were offset by opposing variability from 100–500 m. The net 0–500 m global average temperature warmed by 0.005 °C yr⁻¹. Between 500 and 2,000 m steadier warming averaged 0.002 °C yr⁻¹ with a broad intermediate-depth maximum between 700 and 1,400 m. Most of the heat gain (67 to 98%) occurred in the Southern Hemisphere extratropical ocean. Although this hemispheric asymmetry is consistent with inhomogeneity of radiative forcing⁴ and the greater area of the Southern Hemisphere ocean, ocean dynamics also influence regional patterns of heat gain.

Global ocean sampling of water-column temperature in the twentieth century was spatially and temporally sparse⁵, characterized by strong coverage biases towards the Northern Hemisphere, towards the continental coastlines, and seasonally towards summer. Roughly half a million temperature/salinity profiles to at least 1,000 m were collected by research vessels, mostly in the past 50 years. Additional lower accuracy and shallower temperature-only data have been obtained from commercial and naval vessels. These help to mitigate the coverage deficiencies but raise additional concerns regarding measurement bias errors⁶.

Today the Argo Program² provides systematic coverage of global ocean temperature/salinity from 0–2,000 m using 3,500 autonomous profiling floats spaced about every 3° of latitude and longitude, each providing a temperature/salinity profile every 10 days. Profiling float technology⁷ allows data to be collected without a ship by long-lived free-drifting instruments. Argo has collected 1.2 million temperature/salinity profiles and continues to provide 10,000 profiles per month, with far greater spatial and temporal homogeneity than that achieved historically. Previous investigations of ocean heat content⁵ have combined Argo and historical data of variable quality, and these studies have been impacted by coverage and measurement bias issues. Here we estimate ocean heat gain over the 2006–2013 period for which Argo coverage is global (Methods), and through the exclusive use of Argo data with uniformly high quality.

Argo's ocean temperature data set is invaluable for estimating the net radiation balance of the Earth. The deduced excess of downward over outgoing radiation⁸ driving global warming is too small to measure directly as radiative fluxes⁹. About 93% of this net planetary energy increase is stored in the oceans¹, a result of the large heat capacity of sea water relative to air, the ocean's dominance of the planet's surface area, and the ocean's ability to transport excess heat away from the surface into deep waters. Using historical ocean temperature data together with modern Argo data the increasing heat content of the upper ocean has been estimated to be in the range 0.3 to 0.6 W m⁻², averaged over the area of the Earth, for periods ranging from the past 135 years¹⁰ to the past 50 (refs 11–14), 20 (ref. 15), or 8–12 (refs 16–18) years. These estimates of the rate of ocean heat gain are remarkably similar given the disparate time spans and the potentially large errors due to poor coverage in historical data sets^{9,18,19}. It should be noted that errors in these earlier studies are almost as large as the signal.

Although heat gain is measured by the vertically integrated temperature change through the water column, sea surface temperature (SST) is also of interest because it sets the temperature of the base of the marine atmosphere. Global mean SST has increased by about 0.1 °C decade⁻¹ since 1951 (ref. 20) but has no significant trend for the period 1998–2013. Explanations for the recent 'pause' in SST warming include La Niña-like cooling in the eastern equatorial Pacific²¹, strengthening of the Pacific trade winds²², and tropical latent heat anomalies together with extratropical atmospheric teleconnections²³. However, it is heat gain and not SST that reflects the planetary energy imbalance and thus the warming rate of the climate system. The high variability of the SST record serves to emphasize that it is a poor indicator of the steadier subsurface-ocean and climate warming signal.

As Argo profiles are randomly distributed, spatial and temporal gridding is required. To demonstrate the robust nature of the signals, three contrasting statistical methods of estimating global heat content patterns from raw Argo profiles are used. An optimal interpolation²⁴ (OI) and a robust parametric fit²⁵ (RPF) are applied to temperature profiles and a reduced space optimal interpolation²⁶ (RSOI) is applied to depth-integrated heat content estimates. Further details are provided in the Methods. In each case, we report anomalies from a mean of data from January 2006 to December 2013.

Global mean SST anomalies from 1998 to 2013 in the NOAA (National Oceanic and Atmospheric Administration) OI SST product²⁷ (Fig. 1) illustrate the large interannual variability that characterizes SST and marine atmospheric temperature. There is no significant trend in the time series for either 1998–2013 (the recent

¹ Scripps Institution of Oceanography, University of California, San Diego, California 92075, USA. ² Centre for Australian Weather and Climate Research, CSIRO Oceans and Atmosphere Flagship, Hobart, Tasmania 7000, Australia. ³ National Institute of Water and Atmospheric Research, Wellington 6021, New Zealand. *e-mail: droemmich@ucsd.edu

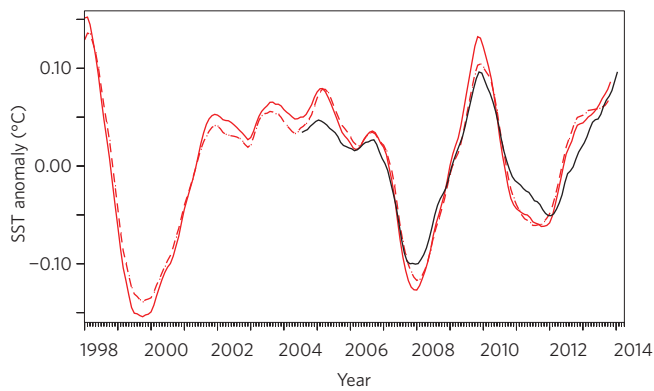


Figure 1 | Globally averaged SST anomaly. 5-m Argo OI temperature (black), NOAA OI SST v2 (ref. 27) masked to the same area as the Argo OI (solid red), NOAA OI SST v2 without the Argo mask (dashed red). All figures are 12-month running means unless otherwise noted.

‘pause’) or 2006–2013 periods. The globally averaged temperature anomaly at 5 m depth from the Argo OI (ref. 24; not used in the NOAA SST product) tracks the SST product closely. As the gridded Argo data set does not include high latitudes, marginal seas, and continental shelves, a more direct comparison of Argo near-surface temperature with the NOAA SST product is made by masking the latter to exclude these same regions (Fig. 1). Differences among the time series show the weak sensitivity in this global metric to Argo’s lack of observations in some regions, such as the Indonesian seas, and to undersampling in others (also Supplementary Figs 1 and 2).

The large interannual variability in global SST anomaly (Fig. 1) is found to track with the upper 100 m of the global ocean temperature anomaly (Fig. 2a). In the deeper 100 to 500 m layer, the anomalies have the opposite sign to those above 100 m except in 2013. The opposing anomalies in the 0–100 and 100–500 m layers are related to El Niño/Southern Oscillation (ENSO) variability in the depth and slope of the equatorial Pacific thermocline³. Below 500 m, a steadier warming over time through the water column is evident (Fig. 2a). The 8-year trend in globally averaged temperature anomaly versus depth (Fig. 2b) illustrates the separation into upper layers with high interannual variability, and therefore large uncertainty in the trend, and deeper steadier warming with lower uncertainty, robust across

the three methods. This illustrates further that, on the timescale observed here, surface temperature is not representative of heat gain by the climate system. The lack of correspondence between surface temperature and net climate heat gain is also seen in climate models²⁸.

The spatial distribution of the heat gain (Fig. 3a) reveals a large build-up of heat in the mid-latitude South Indian and Pacific oceans, with weaker warming in the South Atlantic. Changes in the tropics are weak and show compensation between Pacific cooling and Indian Ocean warming. The North Pacific and North Atlantic show compensating warming and cooling regions with the far North Atlantic warming rate being relatively weak, in contrast to previous decades²⁹. The zonally integrated heat gain (Fig. 3b) confirms the visual assessment of Southern Hemisphere warming and is consistent across the three estimation techniques. The 40° S maximum is near the centre of the deep portion of the subtropical gyres in the three oceans, and the heat gain there, particularly in the South Pacific (Fig. 3a), is consistent with subduction of heat by the mean circulation and a continued strengthening of these gyres³⁰ due to changes in the pattern and strength of mid-latitude westerly winds.

Indeed, much of the interannual variability seen in temperature versus depth (Fig. 2), and in the spatial patterns of heat gain (Fig. 3a), is due to ocean dynamics rather than local air–sea exchanges. For example the offsetting anomalies in depth due to the ENSO wind-driven tilting of the Pacific equatorial thermocline³, or in latitude due to meandering of zonal fronts, as in the North Pacific at 36° N (Fig. 3a), largely indicate redistribution rather than overall changes in heat content. Steadier warming signals are seen by integrating over larger regions and greater depth intervals, for cancellation of offsetting dynamically generated anomalies. Even on oceanic and hemispheric scales, ocean circulation variability, including meridional overturning circulations, may have substantial impacts on regional heat storage²⁹, although decadal meridional overturning circulation variability is poorly known. Only through global measurement can regional oceanic redistributions of heat be averaged out.

Integrating over all of the extratropical Southern Hemisphere oceans, the heat gain estimates range from 3.8 to 7.3 × 10²¹ J yr⁻¹ (Fig. 4a and Table 1), equivalent to 67 to 98% of the respective global totals. There are much weaker trends in the tropics and in the Northern Hemisphere extratropics. The area of the extratropical Southern Hemisphere ocean is twice that of the extratropical

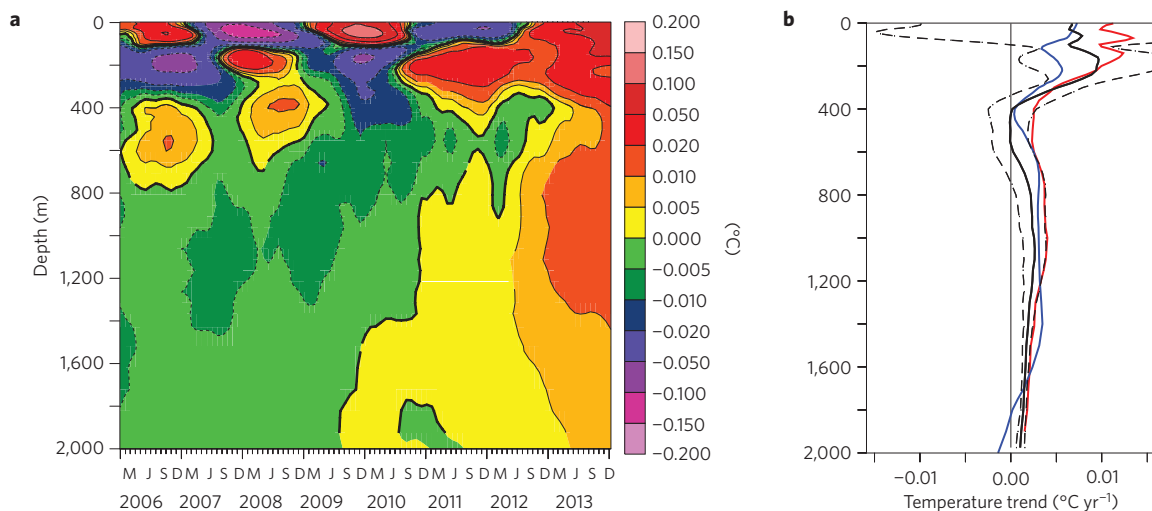


Figure 2 | Depth dependence of temperature change. **a**, Globally averaged temperature anomaly (colour scale) versus depth from the OI (ref. 14) estimate. **b**, Temperature trend versus depth, zonally averaged, for OI (black), RPF (ref. 15; red) and RSOI (ref. 16; dark blue) estimates. The 95% confidence interval (dashed) is shown for the OI alone.

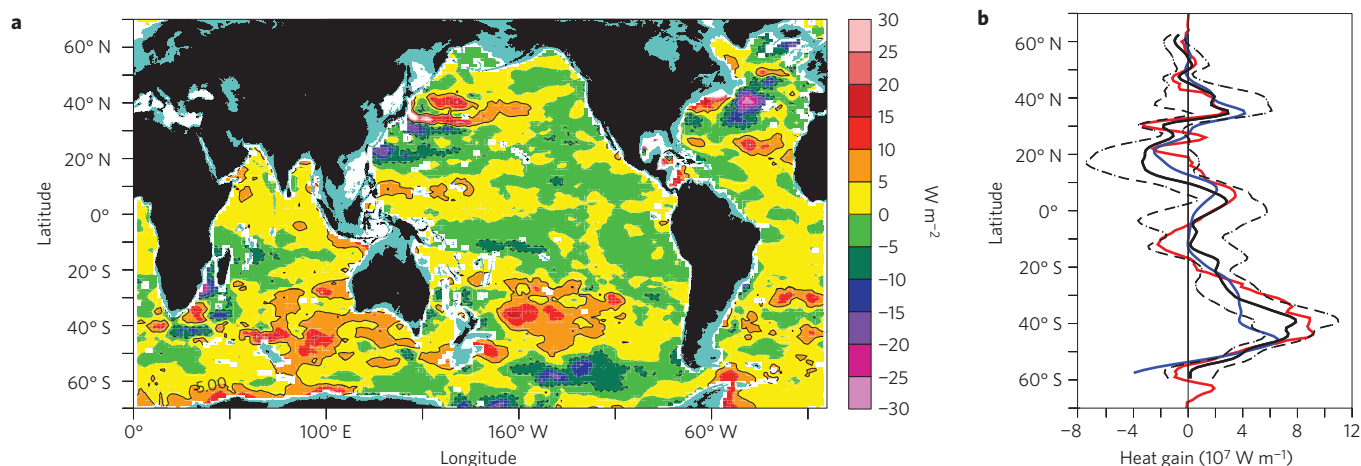


Figure 3 | The spatial pattern of heat gain. **a**, Trend in heat content, 0–2,000 m from the RPF (ref. 15) estimate. A contour line is shown for $\pm 5 \text{ W m}^{-2}$. **b**, Zonally integrated heat gain (10^7 W m^{-1}) versus latitude for OI (black), RPF (red) and RSOI (dark blue) estimates. The 95% confidence interval (dashed) is shown for the OI estimate alone.

Northern Hemisphere ocean, and the large heat gain in the former amounts to a spatial average of 1.5 W m^{-2} (OI estimate) over that ocean region. Estimates of inhomogeneous radiative forcing by aerosols and ozone⁴ indicate a net radiative cooling that is greater in the Northern Hemisphere extratropics than the Southern Hemisphere extratropics by about 1 W m^{-2} . Assuming a weak cross-equatorial ocean heat flux anomaly, this is consistent with the stronger warming observed in the Southern Hemisphere oceans. The predominance of extratropical Southern Hemisphere warming also has been inferred over longer timescales from the 1990s to the Argo era^{29,31}.

Notwithstanding the ‘pause’ in SST warming, the heat content of both the upper 500 m and the 500–2,000 m layers has continued to increase (Fig. 4b), with similar trends for the two depth intervals from 2006 to 2013 of $2.9 \pm 1.3 \times 10^{21} \text{ J yr}^{-1}$ and $2.7 \pm 1.6 \times 10^{21} \text{ J yr}^{-1}$, respectively (OI estimate). This is equivalent to warming rates of about $0.005 \text{ }^\circ\text{C yr}^{-1}$ for 0–500 m and $0.002 \text{ }^\circ\text{C yr}^{-1}$ for 500–2,000 m. The SST ‘pause’ is not an interruption in 0–500 m warming but rather is an aliasing of the longer-term SST trend by the large interannual variability due to ocean vertical heat transport between the 0–100 m and 100–500 m layers³. Warming throughout the 0–500 m layer is observed in 2013 (no cancelling anomalies, Fig. 2a). The vertical structure of the 500–2,000 m warming (Fig. 2b), with a broad maximum between 700 and 1,400 m in the three estimates, implicates the intermediate water layers, Subantarctic Mode Waters and Antarctic Intermediate Waters. These intermediate layers are formed at high southern latitudes, where they are subducted and carry their temperature/salinity properties equatorward via the subtropical gyre interior flows³². Much of the recent heat build-up is occurring in regions where these water masses are formed and pool. At 40° S , a maximum in the zonally averaged temperature trend at 900 m, in the Antarctic Intermediate Water, exceeds $0.01 \text{ }^\circ\text{C yr}^{-1}$.

The estimated trend in global ocean heat content, 0–2,000 m, ranges from 5.6 to $7.9 \times 10^{21} \text{ J yr}^{-1}$ (Table 1 and Fig. 4c), and all three estimates fall within the 95% confidence interval of the OI. Differences are due to the techniques used, for example with the RPF including an explicit estimate of ENSO-related variability, and to a lesser extent to differing spatial domains in the analyses (Supplementary Fig. 3). Normalized by the surface area of Earth (ocean + land), the warming rates range from 0.35 to 0.49 W m^{-2} , consistent with historical estimates^{9–17}. Assuming that the 17% of the ocean area not well sampled by Argo warms at the same rate as the observed 83% (Methods), the total for 0–2,000 m is 0.4 to 0.6 W m^{-2} .

Table 1 | Trend, 2006–2013, in ocean heat content ($10^{21} \text{ J yr}^{-1}$) and 95% confidence interval, for OI, RSOI and RPF estimates.

	OI*	RSOI	RSOI (OI mask) [†]	RPF
Global	5.9 ± 2.6	5.7 ± 2.0	5.6 ± 2.0	7.9 ± 1.2
South of 20° S	5.8 ± 2.0	3.8 ± 1.3	3.9 ± 1.3	7.3 ± 0.6
$20^\circ \text{ S}–20^\circ \text{ N}$	0.4 ± 1.6	1.0 ± 0.9	0.7 ± 1.0	1.9 ± 0.6
North of 20° N	-0.2 ± 1.2	0.9 ± 0.5	1.0 ± 0.6	-1.2 ± 0.7
NH: $0^\circ–60^\circ \text{ N}$	-0.4 ± 1.7	1.6 ± 0.8	1.5 ± 0.7	0.8 ± 0.9
SH: $60^\circ \text{ S}–0^\circ$	6.4 ± 2.3	4.1 ± 1.3	4.2 ± 1.2	7.2 ± 0.8

*OI and RSOI estimates are for time series smoothed with a 12-month running mean. [†]OI mask indicates RSOI estimates integrated over the smaller OI spatial domain. NH, Northern Hemisphere; SH, Southern Hemisphere.

A direct estimate of deep ocean warming for 1990–2010 (ref. 33), based on sparse repeat hydrographic transects, would increase the 0–2,000 m value by $0.07 \pm 0.06 \text{ W m}^{-2}$.

The ability to consistently detect a global upper ocean (0–2,000 m) heat gain of 0.4 to 0.6 W m^{-2} over the short 2006–2013 period is historically unprecedented. Homogeneous global coverage, high data quality, and temporal resolution of seasonal and interannual fluctuations are key attributes for enabling the Argo-only analyses that underpin this result. Further, the consistency among the three different infilling techniques highlights the robustness of the spatial patterns of warming during this period. Only 50% of the warming diagnosed here occurs above 700 m, the depth to which past heat content studies were largely restricted by observing system limitations⁵. The 0–500 m upper ocean warming, with its high interannual variability, is matched by a second maximum at intermediate depths of 700 to 1,400 m, with lower variability. Warming may extend below 2,000 m. Moreover, the present-day global ocean warming signal is dominated by the Southern Hemisphere extratropical latitudes, a result that is influenced by decadal anomalies in ocean circulation, by asymmetry in radiative forcing and by the greater area of the Southern Hemisphere ocean.

The Earth’s energy budget³⁴ closes, with substantial uncertainties, even over the short present-day Argo record. That is, the heat gain in the ocean of 0.4 to 0.6 W m^{-2} is in the range of the difference between the effective radiative forcing (1.1 to 3.3 W m^{-2} downward in 2010 relative to 1750)³⁵ and the radiative response due to the

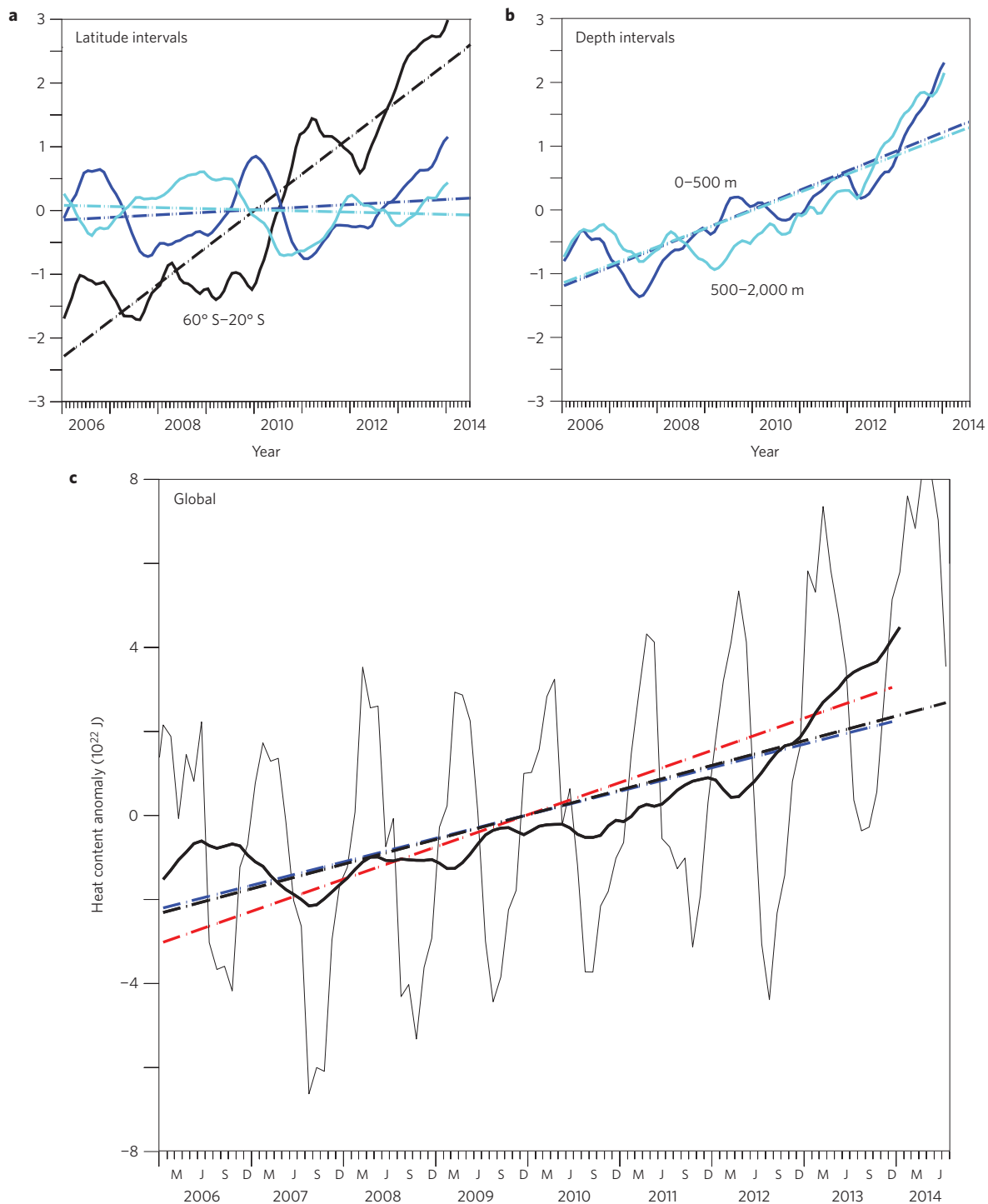


Figure 4 | Global ocean heat gain. **a**, Global heat content anomaly (10^{22} J), OI estimate, for latitude ranges 60° S to 20° S (black), 20° S to 20° N (dark blue), and 20° N to 60° N (light blue), with trends (dashed, same colours). **b**, Heat content anomaly, OI estimate, 0–2,000 m, for depth ranges 0–500 m (dark blue) and 500–2,000 m (light blue), with respective trends (dashed, same colours). **c**, Monthly (unsmoothed) time series of global heat content anomaly from the OI estimate (black, 10^{22} J), 0–2,000 m, with 12-month running mean (thick black) and trend (dashed black). Trends are also shown for the RPF (red) and RSOI (dark blue) estimates.

increase in SST (0.7 to 2.1 W m^{-2} upward; ref. 36), and is better quantified than the radiative terms. As measurements of the Earth radiation budget are relatively accurate for estimation of changes over time but less so for the absolute difference of incoming minus outgoing radiation³⁷, an important step in closing the energy budget is to ‘calibrate’ the net radiation with a period of well-measured global ocean heat uptake⁹. Beginning with the present Argo-only

analyses and going forward with planned enhancements to systematic ocean sampling, it is feasible to quantify the total energy budget of the ocean, reducing uncertainties and accounting for the possible sinks of missing energy^{16,34}, including the deep ocean.

Efforts are underway to extend Argo’s spatial domain towards global coverage, including marginal seas and ice-covered regions. Recent successful deployment of prototype Argo floats sampling

to 6,000 m needs to be followed by systematic Argo coverage of the deep and abyssal oceans. These steps and a longer Argo record will provide accurate estimates of total ocean heat storage and its spatial distribution by ocean, position and depth. The most direct and accurate means of observing energy accumulation in the climate system, and thus tracking this fundamental climate index, is with Argo's thousands of precision thermometers making water-column measurements throughout the world ocean. These rates and patterns of global heat gain will challenge other climate observations and models for comprehensive documentation and better understanding of the coupled climate system.

Methods

The 95% confidence intervals reported in the text and figures measure how well the Argo heat content, 12-month running mean time series, is fitted by a linear trend. Apart from the goodness of fit, three sources of error in the interpolated Argo data set are considered: Argo's less than global spatial domain; Argo's undersampling of some regions within that domain; and systematic pressure errors in Argo measurements.

Examination of float distributions during early years of Argo implementation (Supplementary Fig. 1) shows only a few floats in the Southern Hemisphere by 2003, and large coverage gaps remaining in 2004 and 2005. Coverage-related errors are assessed using satellite sea surface height (SSH) in relation to Argo steric height. SSH changes are due to ocean mass variation as well as to steric change. First, a time series of SSH anomaly³⁸ averaged over the OI domain (Supplementary Fig. 2, red) is similar to that averaged over the global altimetric SSH domain (dashed red). The trends of these time series from 2006–2012, $0.25 \pm 0.09 \text{ cm yr}^{-1}$ and $0.29 \pm 0.08 \text{ cm yr}^{-1}$, are not significantly different, nor are those from the SSH trends over the RPF and RSOI domains. The area of the global ocean ($3.6 \times 10^{14} \text{ m}^2$) is about 20% greater than the area of the OI, RPF and RSOI domains (3.0 , 3.0 and $3.1 \times 10^{14} \text{ m}^2$, respectively, Supplementary Fig. 3). As the SSH increase is similar in gridded and non-gridded regions, the heat content integrals for the OI, RPF and RSOI domains are estimated for the global ocean using the ratio of areas (1.2).

With regard to undersampling, particularly while the Argo array was being implemented, a linear regression estimate of de-trended steric height onto de-trended SSH captures 85% of the variance of interannual SSH from 2006 to 2012 (Supplementary Fig. 2). During 2004–2005 the regression estimate based on steric height is visually poorer. It is concluded that Argo coverage was adequate for estimation of global averages in the period beginning in 2006. Examination of the year-to-year distributions of active Argo floats (Supplementary Fig. 1), and the gaps in the array, reinforces this conclusion.

Drift in Argo pressure sensors³⁹ is measured by sampling atmospheric pressure when the float is on the sea surface, and correcting the profile for this drift. One widely used model of Argo float (APEX) had firmware that truncated negative pressure drifts in a substantial number of floats. Effort by Argo data managers has resulted in labelling of cycles whose pressure offset cannot be corrected owing to this truncation. These cycles are excluded from our analysis (Supplementary Fig. 1) to prevent a time-dependent pressure bias and a resulting bias in heat gain. Of the 1.2 million Argo profiles collected so far, 300,000 were excluded from the OI analysis, including 62,000 for uncorrectable pressure drift, 188,000 for other data quality checks²⁴, and 48,000 for location outside the OI gridded region. Similar quality checks apply to the data used in RPF and RSOI estimates. For assessment of global change it is essential that only high-quality data be included.

In the OI (ref. 24) estimate of global ocean heat content anomaly, the temperature anomaly on a 1° latitude/longitude grid with 58 pressure levels is integrated over the constant volume of the gridded ocean (Supplementary Fig. 3), and multiplied by a mean value of density and specific heat capacity. Values from July 2005 to July 2014 are smoothed with a 12-month running mean to form a 2006–2013 series. The RPF (ref. 25) comprises a mean, a trend, seasonal variability and Southern Oscillation Index response, but constrained to Argo data from January 2006 to December 2013. Temperature trends are converted to heat content using a constant salinity of 34.5.

For the RSOI method²⁶, heat content trends are directly estimated using empirical orthogonal functions derived from gridded satellite SSH. Monthly and 1° grid bin-averaged ocean heat content anomalies are mapped using the weighted least-squares procedure previously applied to sea level⁴⁰ and ocean heat content estimation¹². The mapping is applied to Argo steric and ocean heat content anomalies, defined relative to climatologies based solely on Argo observations spanning the periods 2004–2012 and 2006–2012 (ref. 41), with the reduced space covariance derived from dense satellite altimeter sea level anomalies. Reconstructions are performed for all nominal depth levels taking into account bathymetry, and recombined together to extend solutions to shallower and marginal seas.

Argo data are archived by Argo's Global Data Assembly Center as monthly full data set snapshots with a digital object identifier (DOI) assigned to each.

For the OI analysis, this includes Argo data to July 2014:

<http://dx.doi.org/10.12770/a9acdd12-9d1b-4961-87ae-b935c4dbcb89>.

For the RSOI and RPF analyses, this includes Argo data to December 2013:

<http://dx.doi.org/10.12770/c1f5c810-a4b8-4f12-9531-3452fbaeb206>.

Received 30 August 2014; accepted 31 December 2014;

published online 2 February 2015; corrected online 5 February 2015

References

- Rhein, M. *et al.* in *Climate Change 2013: The Physical Science Basis* (eds Stocker, T. F. *et al.*) 264–265 (IPCC, Cambridge Univ. Press, 2013).
- Gould, J. *et al.* Argo profiling floats bring new era of *in situ* ocean observations. *Eos Trans. AGU* **85**, 185–191 (2004).
- Roemmich, D. & Gilson, J. The global ocean imprint of ENSO. *Geophys. Res. Lett.* **38**, L13606 (2011).
- Shindell, D. T. Inhomogeneous forcing and transient climate sensitivity. *Nature Clim. Change* **4**, 274–277 (2014).
- Abraham, J. P. *et al.* A review of global ocean temperature observations: Implications for ocean heat content estimates and climate change. *Rev. Geophys.* **51**, 450–483 (2013).
- Wijffels, S. E. *et al.* Changing expendable bathythermograph fall rates and their impact on estimates of thermosteric sea level rise. *J. Clim.* **21**, 5657–5672 (2008).
- Davis, R. E., Sherman, J. T. & Dufour, J. Profiling ALACEs and other advances in autonomous subsurface floats. *J. Atmos. Ocean. Technol.* **18**, 982–993 (2001).
- Stephens, G. L. *et al.* An update on Earth's energy balance in light of the latest global observations. *Nature Geosci.* **5**, 691–696 (2012).
- Loeb, N. G. *et al.* Observed changes in top-of-the-atmosphere radiation and upper-ocean heating consistent within uncertainty. *Nature Geosci.* **5**, 110–113 (2012).
- Roemmich, D., Gould, W. J. & Gilson, J. 135 years of global ocean warming between the Challenger Expedition and the Argo Program. *Nature Clim. Change* **2**, 425–428 (2012).
- Levitus, S. *et al.* World ocean heat content and thermosteric sea level change (0–2,000 m) 1955–2010. *Geophys. Res. Lett.* **39**, L10603 (2012).
- Domingues, C. M. *et al.* Improved estimates of upper-ocean warming and multi-decadal sea-level rise. *Nature* **453**, 1090–1093 (2008).
- Ishii, M. & Kimoto, M. Reevaluation of historical ocean heat content variations with time-varying XBT and MBT depth bias corrections. *J. Oceanogr.* **65**, 287–299 (2009).
- Palmer, M. D., Haines, K., Tett, S. F. B. & Ansell, T. J. Isolating the signal of ocean global warming. *Geophys. Res. Lett.* **34**, L23610 (2007).
- Lyman, J. M. *et al.* Robust warming of the global upper ocean. *Nature* **465**, 334–337 (2010).
- Llovel, W., Willis, J. K., Landerer, F. W. & Fukumori, I. Deep-ocean contribution to sea level and energy budget not detectable over the past decade. *Nature Clim. Change* **4**, 1031–1035 (2014).
- Allan, R. P. *et al.* Changes in global net radiative imbalance 1985–2012. *Geophys. Res. Lett.* **41**, 5588–5597 (2014).
- Cheng, L. & Zhu, J. Artifacts in variations of ocean heat content induced by the observation system changes. *Geophys. Res. Lett.* **41**, 7276–7283 (2014).
- Durack, P. J., Gleckler, P. J., Landerer, F. W. & Taylor, K. E. Quantifying underestimates of long-term upper-ocean warming. *Nature Clim. Change* **4**, 999–1005 (2014).
- Flato, G. *et al.* in *Climate Change 2013: The Physical Science Basis* (eds Stocker, T. F. *et al.*) 769–772 (IPCC, Cambridge Univ. Press, 2013).
- Kosaka, Y. & Xie, S. P. Recent global-warming hiatus tied to equatorial Pacific surface cooling. *Nature* **501**, 403–407 (2013).
- England, M. *et al.* Recent intensification of wind-driven circulation in the Pacific and the ongoing warming hiatus. *Nature Clim. Change* **4**, 222–227 (2014).
- Trenberth, K. E., Fasullo, J. T., Branstator, G. & Phillips, A. S. Seasonal aspects of the recent pause in surface warming. *Nature Clim. Change* **4**, 911–916 (2014).
- Roemmich, D. & Gilson, J. The 2004–2008 mean and annual cycle of temperature, salinity, and steric height in the global ocean from the Argo Program. *Prog. Oceanogr.* **82**, 81–100 (2009).
- Durack, P. J. & Wijffels, S. E. Fifty year trends in global ocean salinities and their relationship to broad-scale ocean warming. *J. Clim.* **23**, 4342–4362 (2010).
- Kaplan, A., Kushnir, Y. & Cane, M. A. Reduced space optimal interpolation of historical marine sea level pressure: 1854–1992. *J. Clim.* **13**, 2987–3002 (2000).

27. Reynolds, R., Rayner, N. A., Smith, T. M., Stokes, D. C. & Wang, W. An improved *in situ* and satellite SST analysis for climate. *J. Clim.* **15**, 1609–1625 (2002).
28. Palmer, M. D. & McNeill, D. J. Internal variability of Earth's energy budget simulated by CMIP5 climate models. *Environ. Res. Lett.* **9**, 034016 (2014).
29. Chen, X. & Tung, K.-K. Varying planetary heat sink led to global-warming slowdown and acceleration. *Science* **345**, 897–903 (2014).
30. Roemmich, D. *et al.* Decadal spinup of the South Pacific subtropical gyre. *J. Phys. Oceanogr.* **37**, 162–173 (2007).
31. Sutton, P. & Roemmich, D. Decadal steric and sea surface height changes in the Southern Hemisphere. *Geophys. Res. Lett.* **38**, L08604 (2011).
32. Sloyan, B. & Rintoul, S. Circulation, renewal, and modification of Antarctic Mode and Intermediate Water. *J. Phys. Oceanogr.* **31**, 1005–1030 (2001).
33. Purkey, S. G. & Johnson, G. C. Warming of global abyssal and deep Southern Ocean waters between the 1990s and 2000s: Contributions to global heat and sea level rise budgets. *J. Clim.* **23**, 6336–6351 (2010).
34. Trenberth, K. & Fasullo, J. Tracking Earth's energy. *Science* **328**, 316–317 (2010).
35. Myhre, G. *et al.* in *Climate Change 2013: The Physical Science Basis* (eds Stocker, T. F. *et al.*) Ch. 8 (IPCC, Cambridge Univ. Press, 2013).
36. Church, J. *et al.* in *Climate Change 2013: The Physical Science Basis* (eds Stocker, T. F. *et al.*) Ch. 13 (IPCC, Cambridge Univ. Press, 2013).
37. Trenberth, K. E., Fasullo, J. T. & Balmaseda, M. A. Earth's energy imbalance. *J. Clim.* **27**, 3129–3144 (2014).
38. Ducet, N., Le Traon, P. Y. & Reverdin, G. Global high-resolution mapping of ocean circulation from TOPEX/Poseidon and ERS-1 and -2. *J. Geophys. Res.* **105**, 19477–19498 (2000).
39. Barker, P. M., Dunn, J. R., Domingues, C. M. & Wijffels, S. Pressure sensor drifts in Argo and their impacts. *J. Atmos. Ocean. Technol.* **28**, 1036–1049 (2011).
40. Church, J. A., White, N. J., Coleman, R., Lambeck, K. & Mitrovica, J. X. Estimates of the regional distribution of sea level rise over the 1950–2000 period. *J. Clim.* **17**, 2609–2625 (2004).
41. Ridgway, K. R., Dunn, J. R. & Wilkin, J. L. Ocean interpolation by four-dimensional weighted least squares—Application to the waters around Australasia. *J. Atmos. Ocean. Technol.* **19**, 1357–1375 (2002).

Acknowledgements

The Argo data used here were collected and are made freely available by the International Argo Program and by the national programmes that contribute to it. D.R. and J.G., and their part in the Argo Program, were supported by US. Argo through NOAA Grant NA10OAR4310139 (CIMEC/ SIO Argo). J.C., D.M. and S.W. were partly financially supported by the Australian Climate Change Science Program. NOAA_OL_SST_V2 data were provided by the NOAA/OAR/ESRL PSD, Boulder, Colorado, USA. The satellite altimeter SSH products were provided by AVISO with support from the Centre National d'Etudes Spatiales (CNES).

Author contributions

All co-author (listed alphabetically) contributions were equal, consisting of the three interpolated forms of the Argo data set plus many thoughts, suggestions and revisions improving the manuscript. The first author assembled the interpolated data sets, created the figures and drafted the manuscript.

Additional information

Supplementary information is available in the [online version of the paper](#). Reprints and permissions information is available online at www.nature.com/reprints. Correspondence and requests for materials should be addressed to D.R.

Competing financial interests

The authors declare no competing financial interests.